ELSEVIER

Nuclear Physics A 587 (1995) 318–338

NUCLEAR PHYSICS A

The photodissociation of ^{8}B and the solar neutrino problem

C.A. Bertulani [1]

Gesellschaft für Schwerionenforschung, KPII, Planckstr. 1, D-64291 Darmstadt, Germany

Received 16 September 1994; revised 23 December 1994

Abstract

The extraction of the photodissociation cross sections of ^{8}B from Coulomb dissociation experiments is investigated. A careful study is done on the contributions of the E1, E2 and M1 multipolarities to the breakup. A comparison with the data of a recent experiment is performed. It is shown that the extraction of the radiative capture cross sections ^{7}Be(p,γ)^{8}B which are relevant for the solar neutrino problem is not affected appreciably by Coulomb reacceleration. A non-perturbative model is used for the purpose. Emphasis is put on the perspectives for future experiments which are planned at the University of Notre Dame, RIKEN (Japan) and GSI (Germany). An analysis of the total yields of "photon-point" processes in inelastic electron scattering is also done.

1. Introduction

The solar neutrino problem is related to a factor of two difference between the theoretically calculated and the experimentally measured neutrino flux from the sun. This discrepancy is more accentuated for the measurements of the Homestake [2] and the Kamiokande [3] experiments. The Gallex [4] and SAGE [5] experiments also imply a discrepancy, although more moderate, between theory and experiment. While the Gallex and the SAGE experiments measure neutrinos which are as low in energy as 233 keV, the Homestake and the Kamiokande experiments measure high energy neutrinos. Thus, the discrepancy seems to be larger for the higher neutrino energies.

[1] Present and permanent address: Instituto de Física, Universidade Federal do Rio de Janeiro, 21945-970 Rio de Janeiro, RJ, Brazil.

SSDI 0375-9474(94)00826-4

Most of the high neutrinos ($E_\nu > 2$ MeV) come from the beta-decay of ^{8}B. The main mechanism through which the ^{8}B is produced in the sun is the ^{7}Be(p,γ)^{8}B reaction [1]. If the cross section for this reaction were half of the value which is presently used as an input to the standard solar model [1] the Homestake and the Kamiokande experiments would agree well, although the gallium results would remain unexplained. It is also worthwhile to say that this change might have other implications which can be in disagreement with the SSM model. A proposed solution to the solar neutrino problem is that the discrepancy lies not in the nuclear cross sections that are involved in the determination of the neutrino fluxes, but rather in the behaviour of the neutrinos during their flight to the terrestrial detectors, most likely matter induced oscillations into other neutrino types (the MSW effect [1]) to which the detectors are insensitive. However, not all the nuclear cross sections are known with the desired accuracy, and their inaccuracies will significantly affect the interpretation of the Davis ^{37}Cl (Homestake) and Kamiokande Cherenkov detectors. The reaction ^{7}Be(p,γ)^{8}B accounts for the bulk of the neutrinos seen by ^{37}Cl and is the sole source of neutrinos seen by Kamiokande.

The ^{7}Be(p,γ)^{8}B reaction occurs in the sun at a temperature corresponding to a relative p–^{7}Be energy of about 20 keV. Due to the Coulomb barrier, the magnitude of the cross section at this energy is too small to be measured directly. Direct measurements have been done down to an energy of 120 keV [6]. The measurements of this cross section have always been difficult, because the target is radioactive and relatively short lived (^{7}Be has a halflife of 53 days), and the measurements have been plagued with normalization. Thus, although the most recent and careful experiments of Fillipone et al. [6] have a quoted error of 10%, Barker and Spear [7] argue that the true result may be smaller than that used in the predictions of Bahcall [1], by as much as 30%, due to a combination of normalization, data selection and excitation function uncertainties.

Another controversial point is that the input in the solar models is an extrapolation of the cross section to the 20 keV region. This procedure yields an astrophysical S-factor close to 20 keV·b [9]. These extrapolations are done based on nuclear models which allow some flexibility, and only the experiment can tell how accurate these models are. Therefore, as long as a measurement of the radiative capture cross section for the reaction ^{7}Be(p,γ)^{8}B at low energies is not done, the solar neutrino problem cannot be accepted as solved.

A new technique [10] is now available for the measurements of these cross sections. One studies the inverse reaction $^8\mathrm{B} + \gamma \rightarrow {}^7\mathrm{Be} + \mathrm{p}$ through the Coulomb breakup of ^{8}B on a heavy target. The Coulomb field of the heavy nucleus provides the equivalent photons. The ^{7}Be(p,γ)^{8}B cross section is obtained by detailed balance. This method has been shown to work very well for at least two reactions [11,12] (for a recent review see Ref. [14]). Experiments with real photons are infeasible. But, in first-order, Coulomb excitation involves the same matrix elements as those of photo-induced processes. Furthermore, the coherent field of a large Z nucleus results in very large dissociation cross sections, which can be studied in present experimental facilities [10]. A recent experiment by Motobayashi et al. [13] have used the Coulomb dissociation

method to extract the photodissociation cross section $^8B + \gamma \rightarrow ^7Be + p$.

The main problems with the method are (a) to experimentally separate the nuclear from the Coulomb contribution in the breakup events, and (b) contribution from higher order effects, usually called by reacceleration, or post-acceleration, effects [16–18]. When the nuclear contribution to the breakup cross section is large compared to the Coulomb breakup mechanism for the experimentally measurable kinematical conditions, the method is useless. This is likely to be the case for the breakup of oxygen on nuclear targets, in order to extract the much needed information on the $^{12}C(\alpha,\gamma)^{16}O$ relevant for the helium burning in massive stars [20]. For a comprehensive review on the relevance of the radiative capture reactions in astrophysics see the paper by Fowler [15].

The case of Coulomb breakup of ^8B as a tool to obtain the $^7Be(p,\gamma)^8B$ cross section at low energies has been investigated by many authors recently [13,18–20]. In particular, in Ref. [20] it was shown that the nuclear contribution to the breakup of ^8B is negligible at forward angles below a threshold dictated by the onset of nuclear absorption and diffraction effects. This is a very useful result, since (in contrast to the breakup of oxygen) the much simpler semiclassical description of the Coulomb breakup maybe used.

In this article we consider the Coulomb breakup of ^8B at different bombarding energies, namely 5, 50 and 250 MeV/nucleon, e.g., at the Notre Dame University (USA), RIKEN (Japan) and the GSI (Germany). Radioactive beams of boron can be obtained at these energies at several other labs around the world. The advantage of performing a series of experiments at different bombarding energies is that the multipolarity content of the breakup can be disentangled with more accuracy. This is shown in Section 2.

The reaction $^7Be(p,\gamma)^8B$ is dominated by the electric dipole (E1) multipolarity at very low energies, below the 1^+ resonance at 633 keV. Higher order effects, or Coulomb reacceleration effects, act so as to distort the final relative energy of the fragments after the breakup. In Ref. [20] this problem was studied by means of a classical prescription, based on a Monte Carlo calculation. Typel and Baur [19] have recently studied the same problem within second order time-dependent theory. More recently, Esbensen et al. [21] have shown that while the effect is relevant for the breakup of ^{11}Li projectiles on heavy targets, it is small for the breakup of ^{11}Be and large incident energies.

It has been shown [17,21] that a correct treatment of reacceleration effects can only be accomplished by solving the time-dependent Schrödinger equation non-perturbatively. This is because the reacceleration is an effect related not only to the magnitude of the Coulomb breakup probabilities, which can be small, it is also an effect of distortion (caused by the Coulomb field of the target) on the relative motion between the fragments after the breakup. The absence of such distortions are of vital importance to validate the Coulomb dissociation method. We report in Section 3 a calculation based on the numerical solution of the three-dimensional Schrödinger equation in a potential model for $p+^7Be$. The model used is similar to the one used by Esbensen et al. [21] for the breakup of ^{11}Li and ^{11}Be projectiles. An additional difficulty here is the inclusion of the Coulomb barrier for the $p-^7Be$ relative motion. The results of this non-perturbative model are compared with previous calculations. It is shown that the reacceleration effect

is much smaller than the experimental uncertainties that one achieves in the Coulomb dissociation experiments for the breakup of boron. The relative population of the s, p, d and f waves in the continuum is obtained. We also deduce the angular correlations, useful to separate the multipolarity content of the breakup process. As a byproduct of our calculations several predictions are made which are useful for future experiments.

In Section 4 we show that although the luminosity of electron beams are much higher than the ones obtainable in heavy ion facilities, it is hard to use this advantage to extract the photodissociation cross sections needed for astrophysics from inelastic electron scattering. However, the total yields of target breakup by inelastic electron scattering are not small for ideal experiments. Our conclusions are presented in Section 5.

2. First-order breakup of ^{8}B

The extraction of the radiative capture cross section ^{7}Be(p,γ)^{8}B from Coulomb breakup experiments depends on the validity of the first-order perturbation theory [10]. When this approximation is valid the Coulomb breakup cross sections of ^{8}B into p+^{7}Be in a continuum state with energy E is given by

$$\frac{\mathrm{d}^2\sigma_{\mathrm{C}}}{\mathrm{d}E\,\mathrm{d}\Omega} = \tfrac{8}{5}\mu_{\mathrm{bc}}\frac{1}{(E+Q)^3}\,\mathrm{e}^{-2\pi\eta}\sum_{\pi\lambda}\frac{\mathrm{d}^2 n_{\pi\lambda}}{\mathrm{d}E\,\mathrm{d}\Omega}(E_{\mathrm{x}},\Omega)S_{\pi\lambda}(E), \tag{1}$$

where $E_{\mathrm{x}} = E + Q$ is the excitation energy, Q = 137 MeV is the binding energy of the system, and $S_{\pi\lambda}(E)$ is the astrophysical S-factor for the electric, π = E, or magnetic, π = M, multipolarity of order λ. Detailed balance was used to link the ground state of ^{8}B ($J^\pi = 2^+$) to the proton ($J^\pi = \frac{1}{2}^+$) and the ^{7}Be ($J^\pi = \frac{3}{2}^-$) in the final state. The functions $n_{\pi\lambda}(E_{\mathrm{x}},\Omega)$ are known as the virtual, or equivalent, photon numbers. In Ref. [22] it was shown that one can calculate these quantities for all bombarding energies in the semiclassical approach including the effects of retardation and Coulomb repulsion. This is important since both retardation and the Coulomb recoil of the classical trajectory influence the values of $n_{\pi\lambda}(E_{\mathrm{x}},\Omega)$ at bombarding energies around 50–200 MeV/nucleon. At lower energies retardation plays no role and the results of Ref. [22] reproduce the semiclassical Coulomb excitation theory developed in Ref. [23]. At high energies, the Coulomb recoil is not relevant and the analytical results for the equivalent photon numbers are also reproduced [22].

The differential cross section $\mathrm{d}\sigma_{\mathrm{C}}(E)/\mathrm{d}E$ can also be written in the form of Eq. (1), but with the virtual photon numbers integrated over the scattering angle θ, from zero to a maximum value corresponding to a grazing collision. To display the multipolarity dependence of the equivalent photon numbers (angle integrated) we plot them in Fig. 1 for the E1, E2 and M1 multipolarities, and as a function of the excitation energy E_{x}. A lead target is assumed. We observe that the M1 multipolarity is about a factor 100, 10 and 3 smaller than the E1 multipolarity for bombarding energies of 5, 50 and 250 MeV/nucleon, respectively. This is basically a consequence of the fact that $n_{\mathrm{M1}} \propto (v/c)^2 n_{\mathrm{E1}}$, where v is the projectile velocity. The E2 multipolarity is about 2–3

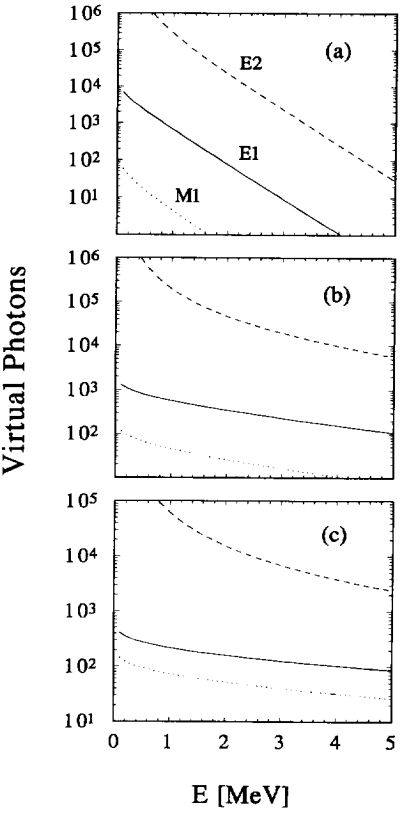

Fig. 1. The multipolarity dependence of the equivalent photon numbers (angle integrated) for the E1 (solid), E2 (dashed) and M1 (dotted) multipolarities, and as a function of the excitation energy E_x. A lead target was assumed. (a), (b) and (c) are for ^{8}B projectiles with bombarding energies of 5, 50 and 250 MeV/nucleon, respectively.

orders of magnitude larger than the E1. This is a reflection of the "tidal" component of a $1/r^2$ force, which is more noticeable for small Fourier components of the field, and small bombarding energies.

The astrophysical S-factors for the ^{7}Be(p,γ)^{8}B reaction is dominated by a 1^+ resonance at E = 633 keV. At lower energies the reaction is dominated by the E1 capture from s and d waves in the continuum. A model calculation by Kim et al. [24] yields an E2 cross section which is a factor 500–1000 smaller than the E1 cross section, over the relevant energy domain. In view of the results presented in Fig. 1 we conclude that the E2 breakup maybe as important as the E1 breakup mode in collisions with the bombarding energies studied here. This fact has been exploited in Ref. [25] to suggest that the data reported by Motobayashi et al. [13] would imply an S_{E1}-factor which is about 30% smaller than what was extracted from the experimental analysis. In view of the potentiality of the Coulomb dissociation method for this particular problem it is important to look at this question more closely.

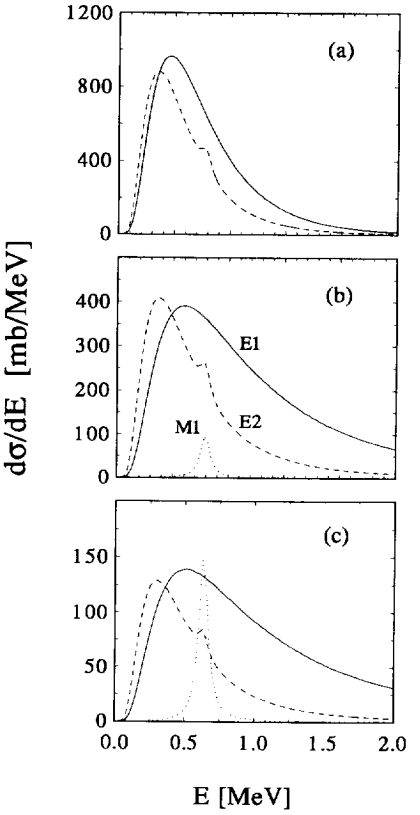

Fig. 2. The energy spectrum of the Coulomb breakup of ^{8}B projectiles on lead at 5 (a), 50 (b) and 250 MeV/nucleon (c) and for the E1, E2 and M1 dissociation modes.

To calculate $d\sigma/dE$ we will use the results of Kim et al. [24] for the astrophysical S-factors of the E1, E2 and M1 capture modes. The M1 and E2 capture modes are influenced by the continuum resonance at 633 keV. This influence is much stronger in the M1 case, so that this capture mode is only relevant for the energy region around 633 keV. In Fig. 2 we plot the energy spectrum of the Coulomb breakup of ^{8}B projectiles on lead at several energies and for the E1, E2 and M1 dissociation modes. Apart from a small resonant component in the E2 dissociation mode, the E1 and E2 contributions to the breakup are dominated by a prominent bump around 300–500 keV in the relative energy of the fragments. This peak is the result of the folding of an increasing function of E, the Sommerfeld penetration factor $\exp\{-2\pi\eta\}$, with a decreasing function of E, the equivalent photon numbers times the $(E+Q)^{-3}$ factor in Eq. (1). It is also clearly seen that the E2 component of the Coulomb breakup is comparable to the E1 component at the region of astrophysical interest ($E < 1$ MeV). However, this result is strongly dependent on the angular kinematical conditions in measurements of the breakup cross sections, and also on the model for the capture cross sections used as input.

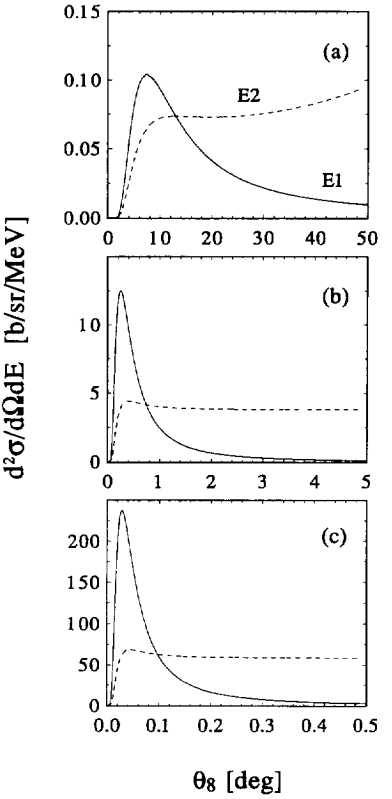

Fig. 3. Angular distribution of the c.m. of p+^{7}Be with a relative energy of 100 keV, and for the E1 and E2 multipolarities. (a), (b) and (c) are for bombarding energies of 5, 50 and 250 MeV/nucleon, respectively.

To show this more clearly we plot in Fig. 3 the angular distribution of the c.m. of the fragments with a relative energy of 100 keV, and for the E1 and E2 multipolarities. A peculiar feature of the angular distribution is that the E1 breakup mode is concentrated at small scattering angles, while the E2 breakup mode is spread over a large angular region. This is more apparent in Fig. 4, for $E = 500$ keV.

This important feature allows one to select events within an angular region and to manipulate the relative contribution of the E2 and E1 components to the breakup. For example, by selecting events for which the scattering occurs below a certain maximum angular value the E2 contribution can be reduced considerably. The calculations of the cross sections presented in Figs. 2–4 were obtained by integrating the equivalent photon numbers in Eq. (1) from $\theta = 0°$ up to θ_S, where θ_S is the grazing scattering angle, above which the strong interaction sets in. These are 75°, 9.4° and 2.5° for $E_{lab} = 5$, 50 and 250 MeV/nucleon, respectively. Let us now assume that in a given experiment one selects events which occur below the angles of 30°, 3° and 0.3° for $E_{lab} = 5$, 50 and 250 MeV/nucleon, respectively. Then the total cross section, integrated over angle and energy, varies considerably and is shown in Table 1. We notice that the E2 contribution is much more affected by the angular limitation of the events than the E1 component.

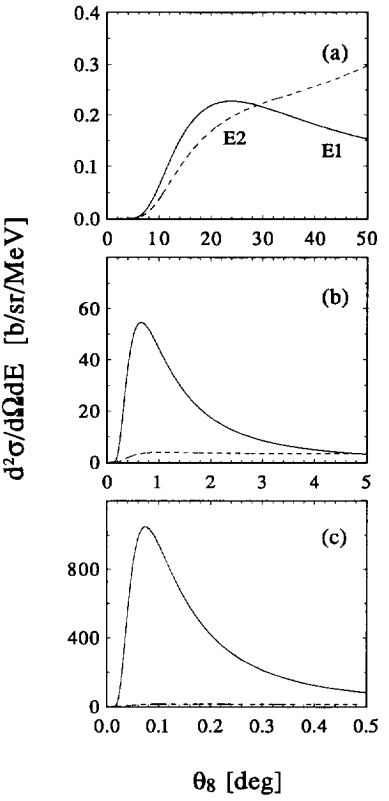

Fig. 4. Same as in Fig. 3, but for E = 500 keV.

We now compare our results with the experiment of Motobayashi et al. [13] for the angular distribution of the breakup of ^{8}B on lead at 46.5 MeV/nucleon. We use the detection efficiency for the data with E_{rel} = 600 keV obtained from the authors [27]. In the experiment the uncertainty of the relative energy of the fragments amounted to 100 keV. Thus, we used as input in the calculations the S-factors averaged over energy bins of 100 keV and the model of Kim et al. [24]. However, for the E1 capture mode we multiplied the results of Kim et al. [24] by a factor so that we could reproduce the

Table 1
E1 and E2 components in the Coulomb breakup of ^{8}B for events below a maximum scattering angle of θ_m = 30°, 3° and 0.3° or θ_S = 75°, 9.4° and 2.5° and at bombarding energies corresponding to 5, 50 and 250 MeV/nucleon, respectively

E_{lab}	$\sigma(\theta < \theta_S)$ [mb]		$\sigma(\theta < \theta_m)$ [mb]	
[MeV/nucl.]	E1	E2	E1	E2
5	572	392	159	73
50	437	210	172	23
250	178	66	38	0.95

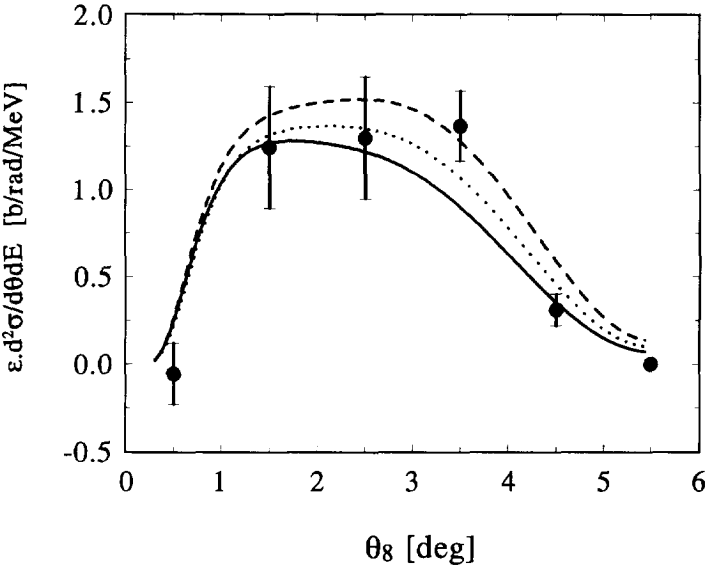

Fig. 5. Angular distribution of the breakup of ^{8}B on lead at 46.5 MeV/nucleon. The data points are from Motobayashi et al. [13]. The solid line is a theoretical calculation for the E1 component folded with the detection efficiency. The dashed and dotted curves include the E2 component with different inputs of the E2 capture in the ^{7}Be(p,γ)^{8}B reaction.

data from Ref. [13]. After this procedure, the effective S_{E1}-factor that we use in our calculations is close to 18 eV·b. Our results are compared with the data of Motobayashi et al. [13] in Fig. 5. The solid line is the breakup cross section multiplied by the detection efficiency assuming only the E1 breakup mode. The dashed line includes the E2 breakup mode. In the experiment of Motobayashi et al. the restriction on the angular distribution of the fragments considerably decreased the effects of the E2 contribution to the breakup. But, if the model of Kim et al. [24] is valid they might not be negligible, as suggested in Ref. [25] and concluded from Fig. 5. However, one must be skeptical about any conclusions related to the E2 contribution in this reaction. The model of Kim et al. [24] has been criticised by Barker [8]. In several other models [8,29,19] the E2 and M1 contribution to the ^{7}Be(p,γ)^{8}B reaction is considerably smaller than the ones predicted by the model of Kim et al. [24]. If we use the model of Typel and Baur [19] for the E2 capture model of the ^{7}Be(p,γ)^{8}B reaction we get the dotted line in Fig. 5, which shows almost no influence of this multipolarity to the data of Ref. [13]. A recent discussion on the contribution of the E2-breakup to the data presented in Fig. 5 has also been published in Refs. [25,26].

We notice that the pattern of the theoretical angular distribution shown in Fig. 5 is slightly different than the one shown in Fig. 2 of Ref. [13], particularly at small angles. A possible explanation is that in Ref. [13] the efficiency curves were obtained by using a theoretical prediction for the dissociation modes as input to a Monte Carlo simulation in which the detection efficiency and the geometry of the detectors were accounted for. This contrasts with the approach used here in which a simple folding

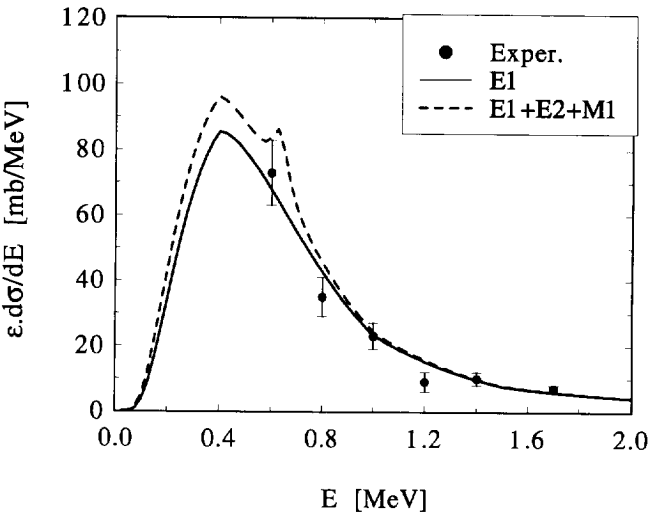

Fig. 6. The energy spectrum of the breakup of ^{8}B on lead at 46.5 MeV/nucleon. The data points are from Motobayashi et al. [13]. The solid line is a theoretical calculation for the E1 component folded with the detection efficiency. The dashed curve include the E2 component using the model of Kim et al. [24] as input for capture cross section ^{7}Be(p,γ)^{8}B.

of the theoretical prediction and the "model dependent" efficiency curve is done. It has also been claimed [28] that the angular averaging is not so simple as treated here, because of the poor experimental resolution and rather large energy bin sizes. It seems that this averaging, with proper inclusion of the detector geometry, has been made more accurately in Ref. [13] with the Monte Carlo simulation.

By switching off the retardation effects in the calculation of the virtual photon numbers [2] which enter Eq. (1) we obtain an average of 3% decrease of the calculated curves presented in Fig. 5, a small effect for this bombarding energy. But, these effects will increase with the bombarding energies and for higher excitation energies, and should be considered in a more detailed analysis of future experiments. For the other (higher) relative energies presented in Ref. [13] we find that the ratio $\sigma(\mathrm{E1}+\mathrm{E2})/\sigma(\mathrm{E1})$ reduces considerably. In view of the discrepancies between the different nuclear models for the ^{7}Be(p,γ)^{8}B reaction we feel that no quantitative conclusions can be drawn about the amount of the M1 and the E2 contribution to the Coulomb breakup of ^{8}B. In fact, the Coulomb dissociation experiments will certainly be very useful to solve this problem, since the several multipolarities contribute differently at different kinematical conditions.

In Fig. 6 the energy spectrum of the breakup yields is shown and compared with the experimental data of Motobayashi et al. [13]. For qualitative comparisons we use the model of Kim et al. [24]. Again, we scale down the E1 capture cross section from Kim et al. [24] which amounts to use a constant factor S_{E1} = 18 eV·b. The solid curve in Fig. 6 is our theoretical calculation (E1 only) folded with the detection

[2] This can be done by neglecting retardation effects in the calculation of the electromagnetic propagator, and on the calculation of the Coulomb trajectory [22].

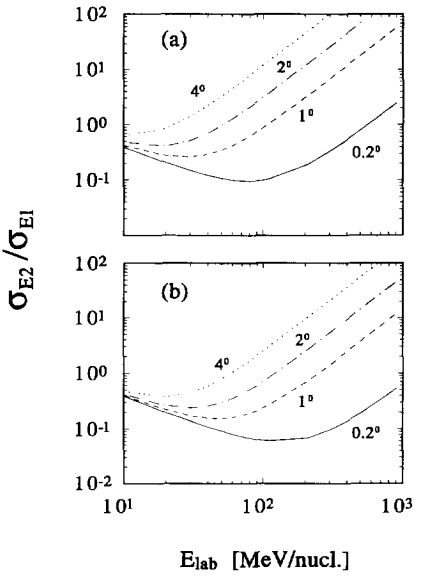

Fig. 7. The ratio σ_{E2}/σ_{E1} as a function of the scattering angle and of the laboratory energy, and for relative energies between the fragments equal to 100 keV (a) and 500 keV (b).

efficiency. The dashed curve includes the E2 contribution to the breakup. In this case the same detection efficiency is used to obtain the E2 component. However, the E2 cross section was integrated only over the angular region where the detection efficiency (Fig. 2 of Ref. [13]) is relevant. As stated before (see Figs. 4 and 5), the exclusion of large angles, reduces considerably the E2 contribution to the breakup data presented in Ref. [13]. Thus, it is not correct to assume the same detection efficiency for the E2 and the E1 breakup mode. If we assume that the E1 and E2 efficiencies are the same, Fig. 6 shows that only the point at 600 keV is appreciably modified by the inclusion of the E2 and of the M1 components. This is basically due to the presence of the 1^+ resonance at 633 keV.

We notice that the S_{E1} = 18 eV·b value used in our calculations contrasts with that used (S_{E1} = 15 eV·b) in the calculation of Ref. [13] and presented in their Fig. 2. The reason for this difference might be due to their different numerical approach, as we discussed above in connection with the angular distribution presented in Fig. 5 (see note added in proof).

In Fig. 7 we show the σ_{E2}/σ_{E1} ratio as a function of the scattering angle, the laboratory energy, and for relative energies between the fragments equal to 100 keV (a) and 500 keV (b). Once again, the model of Kim et al. [24] was used. One sees that the ratio decreases with the relative energy and with scattering angle. The ratio is also smaller for bombarding energies in the range of 10–200 MeV/nucleon. Experiments at different laboratory energies would allow a separation of the relative contributions of the E1 and E2 multipolarities to the breakup.

As stated before, the validity of the Coulomb dissociation method to extract the astrophysical S-factors is strongly dependent on the validity of the first-order perturbation theory. In the next section we present a study of a non-perturbative approach to reacceleration effects.

3. Non-perturbative breakup of ^{8}B

A non-perturbative approach to the study of reacceleration effects was proposed in Refs. [17,21]. In the system of reference of ^{8}B we can write the time-dependent wavefunction for the p+^{7}Be relative motion as

$$\Psi(\boldsymbol{r},t) = \frac{1}{r}\sum_{lm} u_{lm}(\boldsymbol{r},t)Y_{lm}(\hat{\boldsymbol{r}}). \tag{2}$$

Initially the ^{8}B is assumed to be in its bound state. We use a static p+^{7}Be Woods–Saxon nuclear potential which reproduces the binding energy of ^{8}B. The parameters used are $V_0 = -32.65$ MeV, $R = 2.95$ fm and $a = 0.52$ fm for the depth, mean radius and diffusivity of the potential, respectively. The Coulomb potential of a uniform distribution of the ^{7}Be charge with radius $R_C = R$ is added.

We will treat the dynamical problem of the evolution of the wavefunction of the system with a time-dependent Coulomb interaction between the projectile and the target. However, we keep the nuclear potential constant. It is well known that a single set of potential parameters cannot reproduce simultaneously the binding, as well as continuum resonances of a system (see, e.g., the work of Tombrello [30]). But, these are small changes in the potential parameters, and since we are interested here in the reacceleration caused by the time-dependent Coulomb interaction, we will neglect the dynamical modification of the nuclear potential.

For simplicity we will assume that the projectile moves along a straight line. To account for retardation effects we use the Lienard–Wiechert interaction between the target and the projectile [31]. Expanding the interaction in lowest order at the region of the projectile we find that the time-dependent E1 potential is given by

$$V_{E1}(t) = \sqrt{\tfrac{2}{3}\pi}Ze\gamma r\left\{\left[Y_{1,-1}(\boldsymbol{r}) - Y_{11}(\boldsymbol{r})\right]b + \sqrt{2}\,vtY_{10}(\boldsymbol{r})\right\}f(t), \tag{3}$$

where

$$f(t) = \left[b^2 + \gamma^2 v^2 t^2\right]^{-3/2}. \tag{4}$$

In the equations above $\gamma = (1 - v^2/c^2)^{-1/2}$, Z is the target charge, and b is the impact parameter. Eq. (3) is the effective E1 interaction. It is obtained by using the form $(\rho\phi - \boldsymbol{j}\cdot\boldsymbol{A}/c^2)$ for the electromagnetic interaction and the continuity equation to link the magnetic and the electric interactions. This is important for collisions where v/c is not negligible. The effects of retardation is manifest in the appearance of the factors γ in Eq. (3). We will restrict ourselves here to the E1 interaction. But our conclusions will be of general validity and will not be affected by the use of this approximation.

When the expansion (2) and the nuclear plus the time-dependent interaction V_{E1} is inserted in the time-dependent Schrödinger equation a set of coupled differential equations is obtained. The expansion is truncated at $l = 4$, for practical purposes, and the coupled equations is solved numerically. The numerical procedure is similar to that explained in Ref. [17]. For example, if we restrict only to the time-dependent E1 interaction, the equation to be solved is

$$\left[\frac{d^2}{dr^2} - \frac{l(l+1)}{r^2} - \frac{2\mu_{bc}}{\hbar} V_N(r)\right] u_{lm}(r,t)$$
$$- \frac{2\mu_{bc}}{\hbar}\frac{(-1)^m}{\sqrt{2}} f(t) \sum_{l'm'} \sqrt{(2l+1)(2l'+1)} \begin{pmatrix} l & 1 & l' \\ 0 & 0 & 0 \end{pmatrix}$$
$$\times \left\{ ib \left[\begin{pmatrix} l & 1 & l' \\ -m & 1 & m' \end{pmatrix} - \begin{pmatrix} l & 1 & l' \\ -m & -1 & m' \end{pmatrix} \right] + \sqrt{2}\, vt \begin{pmatrix} l & 1 & l' \\ -m & 0 & m' \end{pmatrix} \right\} u_{l'm'}(r,t)$$
$$= -\frac{2\mu_{bc}}{\hbar}\frac{\partial u_{lm}}{\partial t}. \tag{5}$$

This equation couples u_{lm} with neighbouring angular states (due to the discrete values of the Wigner symbols) with $\Delta l = \pm 1$ and $\Delta m = \pm 1, 0$. Including the E2 interaction complicates a bit more the coupled equations, but they are treatable with a truncation in the maximum l-value.

We use a mesh of 1000 points for the coordinate r, with a mesh size of $\Delta r = 0.1$ fm. The time is discretized in a mesh of 800 points with a mesh size of 1 fm/c, starting at $t = -200$ fm/c. As explained in Refs. [17,21], this numerical approach allows one to calculate the time dependence of the wavefunctions and observables useful to study the effects of reacceleration, e.g., occupation probabilities, momentum and energy shifts, etc. We will concentrate here on the results of this numerical approach which are relevant to the ^{8}B breakup. We will first assume a bombarding energy of 50 MeV/nucleon.

The time-dependent wavefunctions computed at 600 fm/c are not influenced by the Coulomb field of the target and are running waves (time-dependent continuum states) added to the remaining part of the ground state wavefunction (which is an $l = 1$ state). The continuum states are obtained by removing the ground-state part of the time-dependent wavefunction, i.e.,

$$\Psi_c = \left[\Psi(t) - \langle\Psi(t)|\Psi_0\rangle\Psi_0\right]\left[1 - |\langle\Psi_0|\Psi(t)\rangle|^2\right]^{-1/2}. \tag{6}$$

In Fig. 8 the probability density of the p+^{7}Be relative motion in the continuum states is plotted as a function of the radial distance, at $t = 400$ fm/c, and for a collision with a lead target with an impact parameter $b = 15$ fm. Also shown is the ground-state wavefunction. One sees that at this time the continuum wavefunction is already far from the range of the static nuclear potential. It contains the characteristic behaviour of a spreading wavepacket.

The wavefunction presented in Fig. 8 is an admixture of several continuum angular momentum states. In Fig. 9 we show the occupation probabilities of different continuum angular momentum states, for a collision with an impact parameter of $b = 15$ and

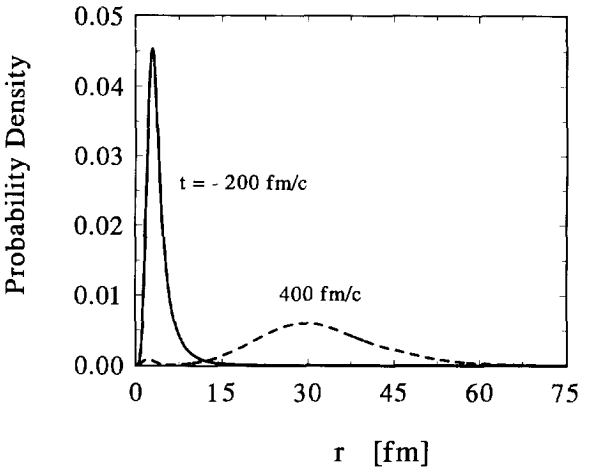

Fig. 8. The probability density of the p+^{7}Be relative motion in the continuum states as a function of the radial distance and at $t = 400$ fm/c. The reaction ^{8}B + Pb at 50 MeV/nucleon is considered.

50 fm, respectively. We observe that at $b = 15$ fm the states are more evenly occupied than at $b = 50$ fm. This occurs because at $b = 15$ fm the interaction is stronger and the continuum–continuum coupling is also stronger. The most relevant states are $l = 0, 1, 2, 3$. At $b = 50$ fm the interaction is weaker, and the continuum–continuum coupling is small. In this case, first order perturbation theory should work well. In fact, at large impact parameters the most occupied states are the s-wave ($l = 0$) and the d-

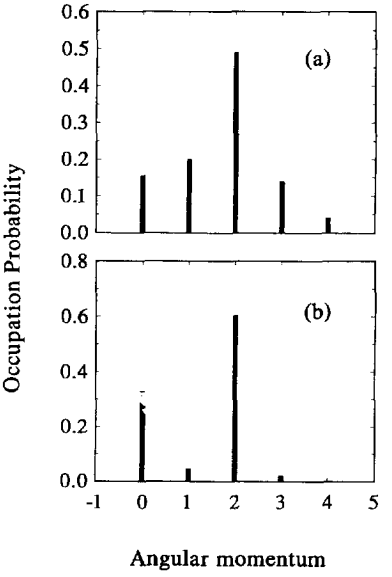

Fig. 9. The occupation probabilities of s ($l = 0$), p ($l = 1$), d ($l = 2$), f ($l = 3$) and g ($l = 4$) waves in the continuum, for a ^{8}B+^{208}Pb collision at 50 MeV/nucleon and an impact parameter of $b = 15$ fm (a) and $b = 50$ fm (b).

wave ($l = 2$) states. These are the same states which are relevant for the dipole capture from the continuum of the p+^{7}Be system [24].

As stated above, of interest here is the comparison between the numerical results with the first-order perturbation theory. Only then we can access the magnitude of the reacceleration effect. In first-order perturbation theory the excitation amplitude is given by

$$a_{\rm fi}(\omega) = \frac{1}{i\hbar}\int_{-\infty}^{\infty} {\rm e}^{i\omega t}\langle {\rm f}|V_{\rm E1}(t)|{\rm i}\rangle, \tag{7}$$

where $\hbar\omega = (E_{\rm f} - E_{\rm i})$ is the excitation energy. The time integrals can be done analytically. The amplitude is proportional to the electric dipole and quadrupole matrix-elements for a transition between the ground state and a continuum state with energy $E = \hbar\omega - Q$. The continuum states are determined numerically for the same nuclear potential. We select the $l = 0$–3 continuum states as input to calculate the matrix elements.

To compare with the non-perturbative calculations, we Fourier transform the time-dependent wavefunction. One gets

$$\Psi_{\rm c}(\boldsymbol{p}) = \sum_{lm} C_{lm}(p) Y_{lm}(\hat{\boldsymbol{p}}), \tag{8}$$

where

$$C_{lm}(p) = \sqrt{\frac{2}{\pi}} i^l \int {\rm d}r\; r j_l(pr) u_{lm}(r,t), \tag{9}$$

where j_l is the spherical Bessel function and $u_{lm}(r,t)$ are the radial continuum wavefunctions, with the ground-state subtracted. The probability density for an excitation to a final state with energy E is directly obtained from the above result. It is

$$\mathcal{P}(b,E,\Omega) = \frac{1}{2}\left(\frac{2m_{\rm bc}}{\hbar^2}\right)^{3/2}\sqrt{E}\,|\Psi_{\rm c}(\boldsymbol{p})|^2. \tag{10}$$

Integrating over Ω we get

$$\mathcal{P}(b,E) = \frac{1}{2}\left(\frac{2m_{\rm bc}}{\hbar^2}\right)^{3/2}\sqrt{E}\sum_{lm}|C_{lm}(p)|^2. \tag{11}$$

The form of the energy spectrum of the relative motion of the fragments in first-order perturbation theory (solid) and in the non-perturbative approach (dashed) is shown in Fig. 10. At small impact parameters the coupling between the continuum states is stronger and the reacceleration effect changes the form of the spectrum. Due to the reacceleration effect higher energy states are populated than in the perturbative calculation. At large impact parameters this effect is smaller, as clearly seen in Fig. 10b.

The average energy of the relative motion can be compared with the results of the first-order perturbation theory. This can be obtained by using Eq. (8) to obtain the first-order energy spectrum and the non-perturbative one described above. Averaging

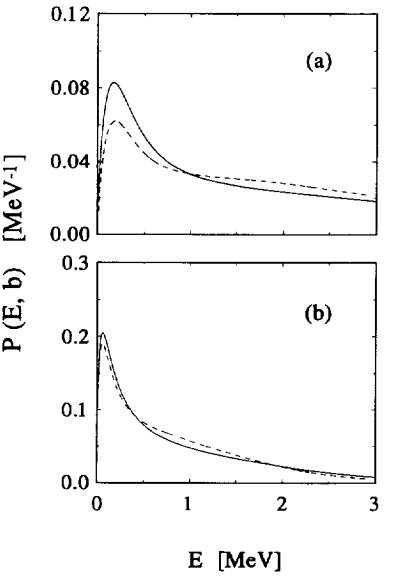

Fig. 10. Energy spectrum of the relative motion of p+^{7}Be in first-order perturbation theory (solid line) and in the non-perturbative approach (dashed) at (a) b = 15 fm and (b) b = 50 fm. A ^{8}B+^{208}Pb collision at 50 MeV/nucleon is assumed.

over impact parameter, the result is shown in Fig. 11 for the ^{8}B+^{208}Pb reaction as a function of the bombarding energy (dashed line).

In Ref. [16] a simple semiclassical model was used to describe the reacceleration effect. Neglecting the binding energy of the (a = b+c) system, the reacceleration causes a shift in the energy of the fragments which is given in the model of Ref. [16] by

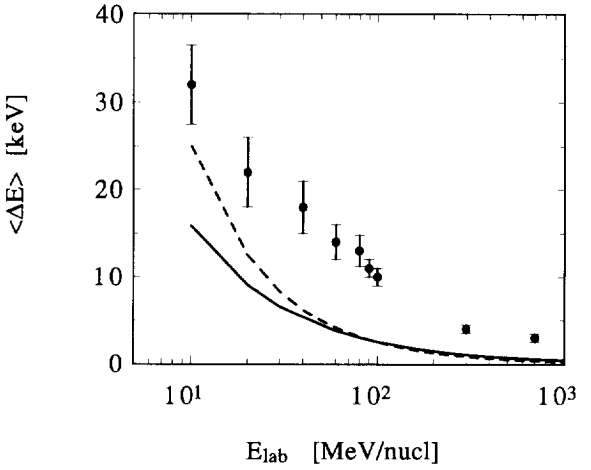

Fig. 11. Total energy associated with the reacceleration effect in the Coulomb breakup ^{8}B on lead targets, as a function of the laboratory energy per nucleon.

$$\Delta E_b = -\Delta E_c = \frac{\pi}{4}\left(\frac{Z_b}{Z_a} - \frac{m_b}{m_a}\right)\frac{Z_a Z e^2}{b}. \tag{12}$$

These energies are much smaller than the beam energy E_{lab}. The energy shifts can thus be calculated as small corrections to the velocities of the fragments. The modification of the final relative motion energy of the fragments due to the reacceleration effect is, in this approximation, equal to

$$\Delta E_{rel} = \tfrac{1}{2}\mu_{bc}(v_b - v_c)^2 \simeq \frac{1}{4}\frac{m_a}{\mu_{bc}}\frac{(\Delta E_b)^2}{E_{lab}}. \tag{13}$$

The results obtained by using this approximation is also shown in Fig. 11 (solid-line) after an average over the impact parameter (this average is weighted by the breakup probabilities, as explained in Ref. [16]). We observe that, despite the very different approaches used, the agreement between the two calculations is quite reasonable. Also shown in Fig. 11 is the Monte Carlo method used in Ref. [20] to calculate the reacceleration energy from a classical prescription (solid circles). The error bars are inherent to numerical accuracy. We see that the numerical approach presented here yields the smallest result for the reacceleration energy (dashed-line). This can be understood as follows. In the approaches of Refs. [16,20] the reacceleration energies were calculated by assuming that the breakup occurs at the distance of closest approach. This overestimates the reacceleration energy, since in a quantum mechanical approach the proton is first brought to the continuum, then tunnels the Coulomb barrier, inducing a time-delay to the reacceleration process. This leads to an effective breakup position which is farther away than the distance of closest approach. This is more critical in the approach used in Ref. [20]. In any case, the reacceleration effect poses no major restriction to the Coulomb dissociation of ^{8}B.

In Ref. [21] it was shown that the reacceleration effects are very important for the breakup of ^{11}Li projectiles on lead at an incident energy of 28 MeV/nucleon. However, it was also shown that the effect is negligible for the breakup of ^{11}Be on lead at 72 MeV/nucleon. This result was ascribed to the higher binding of ^{11}Be and to the smaller effective dipole charge [21]. For the breakup of ^{8}B projectiles, the presence of the Coulomb barrier diminishes further the effect of reacceleration. Our results were obtained using a potential model for p+^{7}Be, similar to that of Kim et al. [24]. As, discussed earlier, this model is thought to be very poor and unreliable [8]. The use of a more refined model for the purpose of calculation of the effects of reacceleration is very difficult and beyond the scope of this work.

Finally, we calculate the angular correlation of the fragments in the frame of reference of the p+^{7}Be. This could be a useful tool to disentangle the E1 from the E2 dissociation mode in future experiments. In our model we can study this effect by varying the impact parameter, since as we have seen in Fig. 9, the occupation probabilities for $L = 1$ and 3 states (accessible also via direct E2 transitions) are also populated via the E1 interaction at small impact parameters. The angular correlation is just proportional to $|\Psi(p)|^2$, obtained from Eqs. (8) and (9). In Fig. 12 we show the angular correlation of the fragments, in the frame of reference of the ^{8}B projectile, for $E = 500$ keV, $\theta = 4°$, a

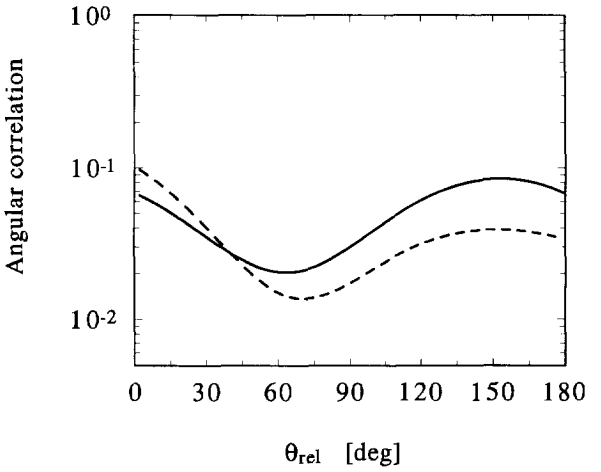

Fig. 12. Angular correlation between the proton and the ^{7}Be-nucleus in their c.m. frame of reference in the Coulomb breakup of ^{8}B on lead at 50 MeV/nucleon and a scattering angle of 4°.

bombarding energy of 50 MeV/nucleon, and $b = 15$ fm (dashed) and $b = 50$ fm (solid). Although small, the occupation of the $l = 1$ and 3 states causes sizeable modification of the angular correlation. The simpler approach of Baur and Weber [32] can be used due to the validity of the first-order perturbation theory.

4. Photodissociation by electron beams

The luminosity of electron beams is so much higher than the ones at heavy ion beam facilities that electron scattering experiments should in principle be another possible tool of obtaining the photodissociation cross sections useful for astrophysical purposes. While such procedure would be useless for the ^{8}B case, it could be useful for other radiative capture reactions of interest, e.g., the $^{12}C(\alpha,\gamma)^{16}O$ reaction.

It is well known that for small momentum transfers electron scattering probes the same matrix elements as in photonuclear experiments (see, e.g, Ref. [33]). The condition is that the four-momentum transfer is much smaller than electron four-momentum (we use now $\hbar = c = 1$), i.e., $q_\mu = (k' - k)_\mu \ll k_\mu$. Also, for forward scattering, the longitudinal momentum transfer is

$$(k' - k)_3 = k\cos\theta - k \simeq k' - k \simeq \frac{E' - E}{v} \simeq \frac{\omega}{c}, \tag{14}$$

where k_3 is the component of the electron momentum along the beam axis. Thus, for the scattering at very forward angles, $q \equiv |\boldsymbol{k}' - \boldsymbol{k}| \simeq \omega/c$, i.e., the momentum transfer is the same as the one by a real photon. Under these circumstances, and in the long-wavelength approximation, both the transverse and the Coulomb matrix elements for inelastic electron scattering are proportional to the electromagnetic matrix elements [33].

It is easy to show that the differential cross section for electron scattering becomes in this limit

$$\frac{d^2\sigma_e}{d\Omega\, d\omega} = \frac{1}{\omega}\sum_{\pi\lambda}\frac{dn_{\pi\lambda}}{d\Omega}\sigma_\gamma^{\pi\lambda}(\omega), \tag{15}$$

where $\sigma_\gamma^{\pi\lambda}$ is the photonuclear cross section, and

$$\frac{dn_{M\lambda}}{d\Omega} = \frac{\alpha}{\pi^2}\left[\frac{EE' - (\hat{\boldsymbol{Q}}\cdot\boldsymbol{k})(\hat{\boldsymbol{Q}}\cdot\boldsymbol{k}') - m^2}{q^4}\right],$$

$$\frac{dn_{E\lambda}}{d\Omega} = \frac{\alpha}{\pi^2}\left\{\left(\frac{\lambda}{\lambda+1}\right)\left[\frac{EE' + \boldsymbol{k}\cdot\boldsymbol{k}' + m^2}{Q^4}\right] + \left[\frac{EE' - (\hat{\boldsymbol{Q}}\cdot\boldsymbol{k})(\hat{\boldsymbol{Q}}\cdot\boldsymbol{k}') - m^2}{q^4}\right]\right\}, \tag{16}$$

where $Q^2 = 2EE'\sin^2(\theta/2)$, $q^2 = Q^2 - \omega^2$ and $\omega = E - E'$.

In order to guess the reaction yields due to the electron scattering at the "photon-point" ($q = \omega$), we integrate the above equations over angles. Since they are a rapidly decreasing function of the scattering angle, we extend the integration to all angles to obtain an upper limit of the photon-point physics in electron accelerators. In this approximation the differential cross section $d\sigma_e/d\omega$ can be expressed in the same form as Eq. (15), but with the total virtual photon numbers given by

$$n_{M\lambda}(\omega) = \frac{2\alpha}{\pi}\left[\ln\xi - \tfrac{1}{2}\right], \qquad n_{E\lambda}(\omega) = \frac{2\alpha}{\pi}\left[\ln\xi - \tfrac{1}{2} + \frac{\lambda}{\lambda+1}\right], \tag{17}$$

where $\xi = 2\gamma E/\omega$.

There are two important differences between this result and the virtual photon numbers that one obtains from Coulomb excitation experiments. Firstly, the virtual photon numbers carry a factor Z^2 due to the coherence effect of all charges in the nucleus. Secondly, the Compton wavelength of a nucleus is much smaller than that of an electron. The "smearing" of the electron wavefunction in the direction perpendicular to the beam weakens the strength of its interaction with the nucleus (see a discussion of this effect in Ref. [31]). Thus, the cross sections for photo-dissociation in electron scattering experiments are much smaller than in Coulomb excitation. This disadvantage could be compensated by means of a large beam luminosity.

The cross section for the reaction $^{16}O(\gamma,\alpha)^{12}C$ is about 3 nb for a relative energy of 1 MeV. Using the Eqs. (18) we get $\sigma_e^{E1} \simeq \sigma_e^{E2} \simeq 1$ nb for CEBAF energies ($E \sim 4$ GeV). For a beam luminosity of 3×10^{38} cm^2/s a considerable number of events can be obtained with a fixed target experiment. However, the extraction of very slow reaction products from the target poses a serious experimental difficulty. Targets of ^{8}B are impossible to construct due to the small lifetime ($\sim$ 700 ms). However, an attempt to use this method to study the $^{12}C(\alpha,\gamma)^{16}O$ would be worthwhile. As shown in Ref. [34], coincidence experiments with the identification of the final products, i.e., the α and/or the oxygen, are quite possible. For astrophysical purposes a triple coincidence measurement is necessary.

5. Conclusions

The Coulomb dissociation of ^{8}B is a promising tool to extract the radiative capture cross section ^{7}Be(p,γ)^{8}B at low energies. The E1 and E2 contribution to the breakup are separable by using proper kinematical conditions. Instead of posing a difficulty, the enhancement of the E2 contribution to the Coulomb breakup at low energies is another useful tool to access information on the relative importance of the many multipolarities which might contribute to a certain radiative capture reaction, and which otherwise can only be extracted from dubious theoretical models.

The effects of reacceleration are small and can be neglected. We have shown this with a series of different approaches, comparing perturbative and non-perturbative methods.

Acknowledgements

I indebted to Drs. H. Esbensen, J. Bahcall and K. Langanke for useful discussions.

Note added in proof

Dr. N. Iwasa has noticed that the input of the ^{7}Be(p,γ)^{8}B cross sections which I have used in my calculations does not exactly correspond the Kim's model. E.g., it underestimates the E2 component for $E_{rel} > 600$ keV and overestimates it for $E_{rel} < 600$ keV. Also, the angular averaging of the detector efficiencies were not used properly. With the inclusion of these modifications, the E2 contribution to the Coulomb dissociation cross section, using Kim's model [24], is about 20% for the cross sections in the energy range of $E_{rel} = 0.6$–1.7 MeV, after folding with the experimental efficiencies. In Kim's model, S_{17} contains about 20% contribution from the non-resonant part of the M1-component. Thus, we can assume, as done in Ref. [13], that the S-factor extracted from the experiment in the energy range $E_{rel} = 0.6$–1.7 MeV is the same as $S_{17}(E) = (E1 + M1)$. Using the energy dependence of $S_{17}(E)$ obtained by Tombrello [30] the data can be fitted with our calculations $(E1 + E2 + M1)$ by scaling down the Trombello's S_{17}-factor by 0.76. This yields a value of S_{17} close to 15 eV·b, in agreement with Ref. [13].

References

[1] J.N. Bahcall, Neutrino astrophysics (Cambridge Univ. Press, New York, 1989).
[2] R. Davis, D.S. Harmer and K.C. Hoffman, Phys. Rev. Lett. 20 (1968) 1205;
R. Davis et al., Proc. 121st Coll. Int. Astr. Union, eds. G. Berthomieu and M. Cribier (Versailles, France, 1989) p. 171.
[3] K.S. Hirata et al., Phys. Rev. Lett. 63 (1989) 16; 65 (1990) 1297; Phys. Rev. D 44 (1991) 2241.
[4] P. Anselmann et al., Phys. Lett. B 285 (1992) 376.
[5] A.I. Abazov et al., Phys. Rev. Lett. 67 (1991) 3332.
[6] B.W. Filippone S.J. Elwyn, C.N. Davis and D.D. Koetke, Phys. Rev. Lett. 50 (1983) 412; Phys. Rev. C 28 (1983) 2222.

[7] F. Barker and R.H. Spear, Ap. J. 307 (1986) 847.
[8] F.C. Barker, Aust. J. Phys. 33 (1980) 177; Phys. Rev. C 37 (1988) 2930.
[9] J.N. Bahcall and M.H. Pinsonneault, Rev. Mod. Phys. 64 (1992) 885.
[10] G. Baur, C.A. Bertulani and H. Rebel, Nucl. Phys. A 458 (1986) 188.
[11] T. Motobayashi et al., Phys. Lett. B 264 (1991) 259.
[12] J. Kiener et al., Phys. Rev. C 44 (1991) 2195.
[13] T. Motobayashi et al., Phys. Rev. Lett. 73 (1994) 2680.
[14] G. Baur and H. Rebel, J. Phys. G 20 (1994) 1.
[15] W. Fowler, Rev. Mod. Phys. 56 (1984) 149.
[16] G. Baur, C.A. Bertulani and D. Kalassa, Nucl. Phys. A 550 (1992) 527.
[17] G. Bertsch and C.A. Bertulani, Nucl. Phys. A 556 (1993) 136; Phys. Rev. C 49 (1994) 2839.
[18] S. Typel and G. Baur, Phys. Rev. C 49 (1994) 379; Nucl. Phys. A 573 (1994) 486.
[19] S. Typel and G. Baur, Phys. Rev. C, in press.
[20] C.A. Bertulani, Phys. Rev. C 49 (1994) 2688.
[21] H. Esbensen, G.F. Bertsch and C.A. Bertulani, Nucl. Phys. A 581 (1995) 107.
[22] A.N.F. Aleixo and C.A. Bertulani, Nucl. Phys. A 505 (1989) 448.
[23] K. Alder and A. Winther, Mat. Fys. Medd. Dan. Vid. Selsk. 31 (1956) 1.
[24] K.H. Kim, M.H. Park and B.T. Kim, Phys. Rev. C 35 (1987) 363.
[25] K. Langanke and T.D. Shoppa, Phys. Rev. 49 (1994) R1771.
[26] M. Gai and C.A. Bertulani, Phys. Rev. C, in press.
[27] M. Gai, private communication.
[28] T. Motobayashi, private communication.
[29] P. Decouvement and D. Baye, Nucl Phys. A 567 (1994) 341.
[30] T.A. Tombrello, Nucl. Phys. A 71 (1965) 459.
[31] J.D. Jackson, Classical electrodynamics (Wiley, New York, 1975).
[32] G. Baur and M. Weber, Nucl. Phys. A 504 (1989) 352.
[33] J. Eisenberg and W. Greiner, Excitation mechanisms of the nuclei (North-Holland, Amsterdam, 1970).
[34] V.F. Dimitrev et al., Nucl. Phys. A 464 (1987) 237.